8442–8455 *Nucleic Acids Research, 2016, Vol. 44, No. 17* *Published online 2 August 2016*
doi: 10.1093/nar/gkw678

YphC and YsxC GTPases assist the maturation of the central protuberance, GTPase associated region and functional core of the 50S ribosomal subunit

Xiaodan Ni[1,2], Joseph H. Davis[3,4], Nikhil Jain[5,6], Aida Razi[1,2], Samir Benlekbir[7], Andrew G. McArthur[1,2], John L. Rubinstein[7,8,9], Robert A. Britton[5,6], James R. Williamson[3,4] and Joaquin Ortega[1,2,*]

[1]Department of Biochemistry and Biomedical Sciences, McMaster University, Hamilton, Ontario L8S4K1, Canada, [2]M.G. DeGroote Institute for Infectious Diseases Research, McMaster University, Hamilton, Ontario L8S4K1, Canada, [3]Department of Molecular Biology, The Scripps Research Institute, La Jolla, CA 92037, USA, [4]Department of Chemistry and The Skaggs Institute for Chemical Biology, The Scripps Research Institute, La Jolla, CA 92037, USA, [5]Department of Molecular Virology and Microbiology, Baylor College of Medicine, Houston, TX 77030, USA, [6]Center for Metagenomics and Microbiome Research, Baylor College of Medicine, Houston, TX 77030, USA, [7]Molecular Structure and Function Program, The Hospital for Sick Children,Toronto, Ontario M5G 0A4, Canada, [8]Department of Biochemistry, University of Toronto, Toronto, Ontario M5S 1A8, Canada and [9]Department of Medical Biophysics, University of Toronto, Toronto, Ontario M5G 1L7, Canada

Received April 12, 2016; Revised July 20, 2016; Accepted July 21, 2016

ABSTRACT

YphC and YsxC are GTPases in *Bacillus subtilis* that facilitate the assembly of the 50S ribosomal subunit, however their roles in this process are still uncharacterized. To explore their function, we used strains in which the only copy of the *yphC* or *ysxC* genes were under the control of an inducible promoter. Under depletion conditions, they accumulated incomplete ribosomal subunits that we named $45S_{YphC}$ and $44.5S_{YsxC}$ particles. Quantitative mass spectrometry analysis and the 5–6 Å resolution cryo-EM maps of the $45S_{YphC}$ and $44.5S_{YsxC}$ particles revealed that the two GTPases participate in the maturation of the central protuberance, GTPase associated region and key RNA helices in the A, P and E functional sites of the 50S subunit. We observed that YphC and YsxC bind specifically to the two immature particles, suggesting that they represent either on-pathway intermediates or that their structure has not significantly diverged from that of the actual substrate. These results describe the nature of these immature particles, a widely used tool to study the assembly process of the ribosome. They also provide the first insights into the function of YphC and YsxC in 50S subunit assembly and are consistent with this process occurring through multiple parallel pathways, as it has been described for the 30S subunit.

INTRODUCTION

A challenge in studying ribosome assembly in bacteria is that cells do not accumulate assembly intermediates. Early studies (1–3) relied on pulse labeling and polyacrylamide gels to study the small amounts of incomplete ribosomal particles that accumulate in normal cells. These experiments identified several 30S and 50S intermediates that overall accounted for only a 2–5% of the total rRNA present in exponentially growing bacteria.

More recently, a few groups have explored the use of small molecule screenings to find chemical inhibitors of specific steps in the ribosome assembly process (4). Small molecules have been extremely effective as precision tools to dissect the translation process performed by the mature ribosome. Many of these small molecules are used as antibiotics and researchers have also used them to capture the conformational changes that mature ribosomes undergo as they decode the mRNA sequence and synthesize the polypeptide chain. However, there are only a handful of chemical probes that inhibit ribosome biogenesis in yeast and mammals (5–9) and only one in bacteria (10). With so few inhibitors available to probe such a complex process, to date ribosome biogenesis has been studied almost exclusively by genetic and biochemical approaches.

A genetic approach that has been popular (11–14) consists of using single gene deletion strains for trans-acting

*To whom correspondence should be addressed. Tel: +1 905 525 9140 (Ext. 22703); Fax: +1 905 522 9033; Email: ortegaj@mcmaster.ca

factors that assist the assembly process of the ribosome. In these strains, the ribosome biogenesis process slows down significantly and it is then possible to isolate and characterize the immature subunits that are the product of the perturbation. Analysis of these particles has provided some of the initial insights into how protein factors assist the assembly process of the ribosomal subunits. For example, characterization of several 30S assembly intermediates that accumulate in *Escherichia coli* cells lacking either YjeQ (11), RimM (12,13) or RbfA (14,15) led to the conclusion that these assembly factors act at the late stages of assembly assisting the maturation of the decoding center of the 30S subunit.

Genetic approaches have also been a prominent experimental tool to establish the function of assembly factors assisting the maturation of the 50S subunit. Of particular interest are three GTPases: RbgA (also known as YlqF), YphC and YsxC. These proteins are essential for growth in *Bacillus subtilis*. Initially, genetic approaches established that the three GTPases act late in the assembly process of the 50S subunit (16–18). More recently (19,20) using a *B. subtilis* strain in which RbgA was under the control of an inducible promoter, it was possible to purify incomplete 50S particles ($45S_{RbgA}$) that accumulated in the cells under depletion conditions for this factor. Characterization of the $45S_{RbgA}$ particles by quantitative mass spectrometry (qMS), cryo-electron microscopy (cryo-EM) and chemical footprinting revealed that RbgA plays a critical role in the maturation of the central protuberance and peptidyl transferase center of the 50S subunit. Importantly, pulse-labeling experiments determined that the $45S_{RbgA}$ particles that accumulate in the cells under RbgA depletion conditions are competent for maturation and progress into functional 70S particles. This finding was important as it provided reassurance that the $45S_{RbgA}$ particles do not represent a dead-end product of the reaction and thus, they render physiologically relevant information about the function of RbgA.

Despite these advances, the mechanistic insights of how RbgA assists the maturation of the functional core of the 50S subunit or the exact functions of the other two GTPases (YphC and YsxC) remain largely unknown. Similarly to RbgA, cells depleted in YphC or YsxC also accumulate incomplete 50S subunits, named $45S_{YphC}$ and $44.5S_{YsxC}$ particles, respectively (17). Therefore, we undertook the analysis of these particles to reveal the function of YphC and YsxC in the assembly of the large ribosomal subunit.

Quantitative mass spectrometry (qMS) analysis revealed that the $45S_{YphC}$ and $44.5S_{YsxC}$ particles lacked several late-binding r-proteins indicating that they represent, as for the $45S_{RbgA}$ particles, late assembly intermediates of the 50S subunit. Cryo-EM reconstructions showed that these particles exhibited significant structural differences with the mature 50S subunit in important functional sites, including the A, P and E sites, central protuberance and GTPase associated region suggesting that YphC and YsxC, together with RbgA, play key roles in the maturation of these regions.

To further investigate the nature of the immature $45S_{RbgA}$, $45S_{YphC}$ and $44.5S_{YsxC}$ particles and determine whether they constitute the actual substrates for the GTPases, we tested the binding of each factor to the immature particles. We found that RbgA, YphC and YsxC can individually bind to each of the immature particles as well as to the mature 50S subunit. This binding is specific as it triggers a stimulation of the intrinsic GTPase activity of the assembly factors. However, a hierarchy of binding similar to that found for bona fide r-proteins was not apparent for the binding of these factors. This finding is consistent with recent kinetic work revealing that assembly of the ribosome occurs through multiple parallel pathways, which introduce the necessary flexibility and redundancy to make ribosome assembly an extremely robust and efficient process. The immature particles also supported binding of multiple assembly factors simultaneously. These results suggest that the assembly intermediates that accumulate in the absence of RbgA, YphC or YsxC are thermodynamically stable. They either constitute the actual substrates for the assembly factors or their conformations have not diverged significantly from that present in the actual substrate, so that RbgA, YphC or YsxC still bind to them.

MATERIALS AND METHODS

Purification of mature 50S subunits and immature $45S_{YphC}$, $45S_{RbgA}$ and $44.5S_{YsxC}$ particles

The mature 50S subunits and immature $45S_{YphC}$, $44.5S_{YsxC}$ and $45S_{RbgA}$ particles were purified from IF2-depleted (RB419), YphC-depleted (RB290), YsxC-depleted (RB260) and RbgA-depleted (RB301) *B. subtilis* strains, respectively. Generation of these strains has been previously described (17,21). The mature 50S subunit and immature $45S_{RbgA}$ particles were purified as described previously (19). The $44.5S_{YsxC}$ and $45S_{YphC}$ particles were purified by the same procedure used with the $45S_{RbgA}$ particles.

Protein overexpression clones

The pET21b-*ylqF* plasmid used to overexpress RbgA was expressed with a C-terminal His_6-tag was generated as described previously (16). The pET15b-*yphC* and pET15b-*ysxC* plasmids used to overexpress YphC and YsxC with a N-terminal His_6 tag cleavable by thrombin protease were produced as follows. The sequence of the *yphC* gene (NCBI reference sequence: NC_000964.3) and *ysxC* gene (NCBI reference sequence: NC_016047.1) were optimized for overexpression in *E. coli* cells using the GeneOptimizer software® and subsequently synthesized (Life Technologies; Thermo Fisher Scientific) with a NdeI and a BamHI site in the 5′ and 3′ ends of the gene, respectively. The genes were cloned into the carrier pMA-RQ (ampR) plasmid using the *SfiI* and *SfiI* cloning sites and subsequently subcloned into the final expression vector pET15b using the NdeI and a BamHI restriction sites. The final constructs were verified by sequencing (MOBIX, McMaster University).

Protein overexpression and purification

YphC and YsxC were overexpressed as N-terminal His_6-tag proteins by transforming *E. coli* BL21 (DE3) with pET15b-*yphC* and pET15b-*ysxC* plasmids, respectively. For both proteins, one liter of LB medium containing 100 μg/ml ampicillin was inoculated with 10 ml of saturated overnight

culture and cells were grown to OD_{600} = 0.6 by incubation at 37°C and shaking at 225 rpm in an Excella E24 incubator (New Brunswick). Expression was induced by the addition of 1mM isopropyl β-D-1-thiogalactopyranoside (IPTG). Cells were then induced for 3 h at 37°C and harvested by centrifugation at 3700*g* for 15 min. Cell pellets were washed with 1 × phosphate-buffered saline (PBS) buffer (137 mM NaCl, 2.7 mM KCl, 8.1 mM Na_2HPO_4 at pH 7.4) and re-suspended in 20 ml of binding buffer containing 50 mM $NaPO_4$ pH 8 and 0.3 M NaCl containing a protease inhibitor cocktail (Complete Protease Inhibitor Cocktail Tablets. Roche). The cell suspension was passed through a French press at 20 000 lb/in^2 pressure three consecutive times and the lysate was spun at 30 000*g* for 45 min to clear cell debris, then filtered with a 0.45 μm filter and loaded into a HiTrap Metal Chelating Column (GE Healthcare Life Sciences) previously equilibrated with binding buffer. Nonspecifically bound proteins were washed with buffer containing 20 mM $NaPO_4$ pH 7.5, 0.5M NaCl and 60 mM imidazole. Elution of YphC and YsxC was done by increasing the concentration of imidazole to 250 mM. Purity of the fractions was assayed by SDS-PAGE and fractions containing each respective protein were collected, pooled together and dialyzed overnight against 20 mM $NaPO_4$ pH 7.5 and 5% glycerol. Dialyzed protein preparations were centrifuged at 12 000*g* for 10 min in an Eppendorf Mini-spin centrifuge to remove any precipitated protein. The N-terminal His_6-tags of YphC and YsxC were removed by digestion with thrombin (Sigma) that was added in the amount of 25 U/ml to the pooled fractions containing the target proteins during dialysis. The reaction mixtures were then loaded onto a Hi-Trap Q HP anion exchange column (GE Healthcare Life Sciences) for YphC protein and Hi-Trap SP HP column (GE Healthcare Life Sciences) for YsxC protein. The columns were pre-equilibrated with Buffer A (20 mM $NaPO_4$ pH 7.5, 5% glycerol). A linear gradient of NaCl concentration from 0 mM and 1 M was used to wash and elute the protein. YphC and YsxC were eluted at a concentration of 350 and 500 mM NaCl, respectively. Protein-containing fractions were verified by SDS-PAGE, concentrated, and NaCl was removed by exchanging the buffer to desalting buffer (50 mM Tris–HCl (pH 7.5), 750 mM KCl, 5 mM $MgCl_2$, 20 mM imidazole, 2 mM DTT and 10% glycerol) using a 10 kDa-cutoff centrifuged concentrator (Amicon). In the final step of concentration the buffer was exchanged to storage buffer (50 mM Tris–HCl at pH 7.5, 750 mM KCl, 5 mM $MgCl_2$, 2 mM DTT and 10% glycerol) also using a 10 kDa-cutoff centrifuged concentrator (Amicon). Pure proteins were frozen in liquid nitrogen and stored at −80°C.

RbgA was overexpressed as a C-terminal His_6-tag protein by transforming *E. coli* BL21 (DE3) with the pET21b-*ylqF* plasmid. The overexpression and purification protocol for RbgA was identical to that used for YphC and YsxC. However, RbgA only required a HiTrap Metal Chelating Column (GE Healthcare Life Sciences) to be purified. There were also the following differences in the buffers used for the purification: the binding buffer used in this case contained 20 mM $NaPO_4$ pH 7.5, 0.5 M NaCl and 20 mM imidazole. The washing buffer for the HiTrap Metal Chelating Column was 20 mM $NaPO_4$ pH 7.5, 0.5 M NaCl and 60 mM imidazole. The protein eluted at a concentration of 250 mM imidazole. The fractions containing RbgA were pooled and dialyzed against buffer containing 20 mM $NaPO_4$ pH 7.5 and 5% glycerol. The C-terminal His_6-tag in RbgA was not removable.

Binding assays

Binding assays were done using a previously published protocol but with modifications (22). In particular, Nanosep Omega centrifugal devices (PALL) (100 kDa cut-off) were prepared by blocking for non-specific binding of proteins by incubating the filter membrane with 500 μl of 1% [w/v] bovine serum albumin (BSA) for 90 min. Filters were then washed by rinsing with 500 μl of RNase free water and then removing any residual blocking solution by adding 500 μl of RNase free water and spinning at 12 000*g* for 10 min. Binding reactions were prepared by incubating 200 pmoles of each assembly factor with 40 pmol of mature or immature ribosomal particles in a 100 μl reaction in Binding Buffer (10 mM Tris–HCl at pH 7.5, 7 mM magnesium acetate, 150 mM NH_4Cl and 1 mM DTT). GTP, GDP and GMPPNP was added in the reactions as indicated at a final concentration of 1 mM. Reactions were incubated at 37°C for 30 min followed by centrifugation in the 100 kDa centrifugal devices at 12 000*g* for 10 min to separate ribosomal particles and bound factors that were retained by the filter from unbound proteins in the flow-through (FT) fraction. The flow-through was collected and the filter was gently washed twice with 100 μl of Binding Buffer followed by a 5 min spin at 12 000*g*. Finally, the ribosomal particles and bound proteins retained by the filter were vigorously resuspended in 100 μl of Binding Buffer and collected as the bound fraction (B). To resolve the flow-through and bound fractions, 30 μl of sample were mixed with 6× SDS-PAGE loading buffer and loaded into a 4–12% Criterion™ XT Bis–Tris gel (Bio-Rad). Samples were run in XT MOPS buffer (Bio-Rad). Gels were stained with Coomassie Brilliant Blue and visualized using a ChemiDoc MP system (Bio-Rad).

Quantitative mass spectrometry

Samples were purified as described above with either 500 mM (high salt) or 150 mM (low salt) NH_4Cl present during the sucrose cushion centrifugation. For the low salt samples, 10 pmol of each sample (50S, $45S_{RbgA}$, $45S_{YphC}$ or $44.5S_{YxsC}$) was spiked with 10 pmol of 70S particles purified from wild-type cells grown in ^{15}N-labeled media as described previously (19). Samples were then precipitated, reduced, alkylated, and digested to tryptic peptides according to Jomaa *et al.* (19). Peptides were injected onto a C18 nanoflex column (Eksigent), and eluted using a 120 min 5–45% convex acetonitrile gradient.

Data was initially collected in a data-dependent acquisition mode with a cycle consisting of a 200 ms MS^1 scan followed by 30 100 ms MS^2 scans, selecting precursors exceeding 125 counts per second. Precursors were excluded for 12 s after their being selected twice. Datasets were searched against the *B. subtilis* proteome using Mascot. Search results were combined to generate a spectral library using Skyline (23).

Data was also collected in a data-independent SWATH acquisition mode (24), using a 250 ms MS^1 scan followed by 32 MS^2 scans ranging 400–1200 Th, each 25 Th in width. Using the spectral library noted above, product ion chromatograms from the SWATH acquisition were extracted for ^{14}N and ^{15}N species using Skyline. Peptides and transitions were filtered to eliminate spectral interference and poorly ionized precursors. $^{14}N/^{15}N$ abundance ratios were calculated for each transition. Protein abundance was calculated as the median value of this ratio, normalized to the median value observed for protein L20, which was expected to be bound stoichiometrically.

Samples undergoing the high salt wash were spiked with a mixture of ^{14}N- and ^{15}N-labeled 70s particles as described (25), and peptide abundances were determined from MS^1 data obtained on an Agilent G1969A ESI-TOF mass spectrometer according to Gulati *et al.* (25). Protein abundance was again calculated as the median $^{14}N/^{15}N$ ratio, normalized to that of protein L20.

GTPase assays

To measure intrinsic GTPase activity, RbgA and YsxC were incubated at a concentration of 2 μM with a range of GTP concentrations (0–1 mM). YphC in equivalent reactions was added to a concentration of 200 nM. The background of the assay itself was measured by running control reactions with no enzyme at each GTP concentration. These background values were subtracted from the total GTPase activity exhibited by the reactions containing the assembly factor at each GTP concentration. To determine the stimulation of RbgA, YsxC and YphC GTPase activity by the ribosomal particles, we assembled reactions containing 50 nM concentration of assembly factor and an equal concentration of either mature 50S subunits or one of the immature particles. All assays were performed by first calculating the background GTPase activity from each ribosomal particle (50S subunit, $45S_{YphC}$, $44.5S_{YsxC}$ and $45S_{RbgA}$ particles) at 50 nM incubated from 0 to 1 mM of GTP. This background subtraction ensured accuracy in the calculations by removing all background phosphate production not due to the assembly factors themselves.

All reactions were incubated at 37°C for 30 min before measuring the released free phosphate by the malachite green assay (BioAssays Systems). The assay showed a linear behaviour for this incubation time. Reactions were performed in the reaction buffer (50 mM Tris–HCl (pH 7.5), 200 mM KCl, 10 mM $MgCl_2$ and 1 mM DTT) and terminated by the addition of malachite green reagent. Released phosphate was detected by monitoring the color formation at 620 nm using a 96-well plate reader (Tecan Sunrise). The apparent K_M and k_{cat} values were calculated by fitting the data to the Michaelis-Menten equation with non-linear regression using the GraphPad Prism software. All these assays were performed at least in triplicate and with at minimum of two different preparations of the assembly factors and ribosomal particles.

Cryo-electron microscopy and image processing

Purified ribosomal particles ($45S_{YphC}$, $44.5S_{YsxC}$) were diluted to a concentration of 40–50 nM in buffer E (10 mM Tris–HCl at pH 7.5, 10 mM magnesium acetate, 60 mM NH_4Cl and 3 mM 2-mercaptoethanol). Approximately 3.6 μl of the diluted sample was applied in the holey carbon grids (c-flat CF-2/2-2C-T) with an additional layer of continuous thin carbon (5–10 nm). Before the sample was applied, grids were glow discharged in air at 5 mA for 15 s. Vitrification of samples was performed in a Vitrobot (FEI) by blotting the grids twice, 15 s each time and with an offset of −1.5 before they were plunged into liquid ethane.

Grids were loaded in a Gatan 626 single tilt cryo-holder and introduced into a FEI Tecnai F20 electron microscope operated at 200 kV and equipped with a Gatan K2 Summit direct detector device camera. This detector was used in counting movie mode with five electrons per pixel per second for 15 seconds exposures and 0.5 s/frame. This method produced movies consisting of 30 frames with an exposure rate of ∼1 $e^-/Å^2$. Movies were collected with a defocus range of 1–2.5 μm and a nominal magnification of 25 000×, which produced images with a calibrated pixel size of 1.45 Å.

The 30 frames in each movie were aligned using the program alignframesleastsquares_list (26) and averaged into one single micrograph with the shiftframes_list program (26). These programs are available from (https://sites.google.com/site/rubinsteingroup/home). These micrographs were used to estimate the parameters of the contrast transfer function using CTFFIND3 (27) and also to determine the coordinates for particles in the frames of the movies. This last step was performed using the autopicking procedure in Relion (28). The coordinates obtained were used to extract candidate particle images from the 30 unaligned frames in the movie. The motion of the individual particles in the frames was tracked and corrected using alignparts_lmbfgs algorithm (26). This procedure produced one stack of particle images fully corrected from beam-induced motion from the first 20 frames of each movie. Therefore, the total accumulated dose to produce these particles images was 20 $e^-/Å^2$. The initial number of particle images in the data sets for the $45S_{YphC}$ and $44.5S_{YsxC}$ structures was 105 302 and 91 724, respectively. These particle data sets were subjected to two- and three-dimensional classification with Relion (28). In the case of the $45S_{YphC}$ particle three-dimensional classes were built from 101 264 particle images and the 45 369 particles assigned to one class were used to build the final consensus 3D map. A similar approach was followed with the $44.5S_{YsxC}$ structure where three-dimensional classes were produced from 87 684 particle images. The final three-dimensional consensus map for the class I conformation was built from the 36 033 particle images that were assigned to one of the 3D classes obtained in the 3D classification and the consensus class II map was produced from the 46 430 particle images from another of the 3D classes.

Subsequently, the data sets producing the consensus structures were subjected to focus classification with subtraction of the residual signal using Relion (28) following an approach previously described (29). The mask for focus classification on the central protuberance, helix 38, GTPase associated region and A, P and E functional sites was generated by converting the atomic model of the 50S subunit (PDB ID 3j9w) into a density map after the following mo-

tifs were removed from the atomic model: 5S rRNA, helices from the 23S rRNA including h80-88 (nt 2280–2420), h38 (nt 890–980), h42-44 (nt 1080–1160), h89-93 (nt 2480–2630), h68-71 (nt 1870–2000), h76-78 (2140-2200), and ribosomal proteins uL16, bL27, uL6, bL33, bL35, bL28, bL36, bL31, uL18, uL5, uL30, uL15, uL10 and uL11. This density map was used to create a soft-edged mask and to also subtract the signal of the mature motifs in the experimental particles. The newly created stacks of particles after signal subtraction and the mask were used as input for the focus classification run. During the classification step, we kept all orientations fixed at the values determined in the refinement of the consensus maps. Each data set rendered three distinct classes that were subjected to a separate 3D auto-refinement using the cryo-EM structure of the 50S subunit from *B. subtilis* (PDB ID 3j9w) low pass filtered to 50 Å.

Prior to visualization, sharpening of the cryo-EM maps was done by applying a negative *B*-factor estimated using automated procedures (30). Relion processes were calculated using the SciNet cluster (31) and a VMWare-based Ubuntu linux server with 32 processors / 256 GB RAM within the McMaster Service Lab and Repository (MSLR) computing cluster. We used the program ResMap (32) to estimate the local resolution of the structures. The UCSF Chimera program (33) was used for the visualization of cryo-EM maps and render figures. To identify the rRNA helices in the $45S_{YphC}$ and $44.5S_{YsxC}$ structures that were different from the mature 50S subunit the atomic model of the *B. subtilis* 50S subunit (PDB ID 3J9W) was docked into the cryo-EM maps first as a rigid body using Chimera and then the fitting was optimized by Molecular Dynamics Flexible Fitting (MDFF) (34).

RESULTS

The $45S_{YphC}$, $44.5S_{YsxC}$ particles represent late assembly intermediates

Depletion of YphC or YsxC in *B. subtilis* cells results in the accumulation of altered large ribosomal subunits (17) that we called $45S_{YphC}$ and $44.5S_{YsxC}$ (Supplementary Figure S1). To purify these particles, we used strains with a single copy of the *yphC* or *ysxC* genes under the control of an IPTG-inducible promoter (17). In the presence of the inducer, lysates from these strains fractionated by sucrose density gradient ultracentrifugation produced ribosome profiles that were indistinguishable from those of wild type cells (17). However, the absence of IPTG produced a drastic reduction in the level of 70S and the accumulation of $45S_{YphC}$ and $44.5S_{YsxC}$ particles that we purified (Supplementary Figure S1). In addition, we also purified mature 50S subunits (Supplementary Figure S1) and $45S_{RbgA}$ particles as we previously described (19).

To determine the protein complement of the three immature particles ($45S_{YphC}$, $44.5S_{YsxC}$ and $44.5S_{RbgA}$) and the mature 50S subunit all cells were grown in ^{14}N-labeled media. The purified particles from these cells were then mixed with a reference spike containing a fixed concentration of ^{15}N-labeled 70S ribosomes and we measured their protein levels relative to this spike using qMS. This analysis showed that r-proteins uL16, bL28 and bL35 (r-protein nomenclature according to Ban *et al.* (35)) were severely depleted (occupancy < 0.25), and that bL27, bL33 and bL36 were significantly depleted (occupancy > 0.25) from all three 45S particles (Figure 1A; orange and purple, respectively). No peptides were found for bL34 in our analysis for any of the samples, thus the occupancy level for this r-protein remained uncharacterized. The mature 50S subunits exhibited a full complement and no signs of depletion for any of these r-proteins. This control experiment confirmed that the buffers used for particle purification and mass spectrometry analysis were not the cause of any of the depletions observed for the other six r-proteins. To determine the effect of NH_4Cl on r-protein association, these assays were performed in duplicate with particles purified either under low (150 mM) or high (500 mM) salt conditions. Interestingly, purification under high salt conditions led to similar occupancy profiles, with depleted proteins exhibiting even lower abundance (Figure 1B).

uL16, bL27, bL28, bL33, bL35 and bL36 are all r-proteins that bind late in 50S subunit reconstitution experiments (36–40). Therefore, we concluded from this analysis that the $45S_{YphC}$, $44.5S_{YsxC}$ particles, similar to the $45S_{RbgA}$ particles, represent late assembly intermediates.

The immature particles accumulating in the YphC and YsxC-depleted cells exhibit multiple conformations

Perhaps the most remarkable finding of the qMS analysis was the fact that the depletion pattern of the $45S_{YphC}$, $44.5S_{YsxC}$ and $45S_{RbgA}$ particles is identical. This result led us to investigate the structural similarity between the three particles and whether the function of YphC and YsxC could be inferred from the structures of the $45S_{YphC}$ and $44.5S_{YsxC}$.

To this end, purified $45S_{YphC}$ and $44.5S_{YsxC}$ particles were imaged by cryo-EM (Supplementary Figure S2; top panels) with a direct detector device camera allowing for full-correction of the beam-induced motion that the ribosomal particles experienced during the image acquisition process (Supplementary Figure S2; bottom panels). Three-dimensional classification of the $45S_{YphC}$ data set using the entire signal in the particle images revealed one distinct three-dimensional class. However, the $44.5S_{YsxC}$ particles exhibited two three-dimensional classes (Figure 2A and B). The percentages of the images assigned to class I and II were 44% and 56%, respectively. The most striking structural differences between the three maps representing the immature particles and the mature 50S subunit structure were in the A, P and E sites. The central protuberance and region nearby the bL7/L12 stalk also differed substantially from the mature subunit (Figure 2A) suggesting that this motif and the functional sites of the subunit are still in an immature state. However, the core of the subunit resembled closely the conformation of the mature 50S subunit (Supplementary Figure S3).

Consistently with the qMS data (Figure 1), the six r-proteins that were found severely depleted in the immature particles (uL16, bL27, bL28, bL33, bL35 and bL36) were all also missing from the cryo-EM maps of the $45S_{YphC}$ and $44.5S_{YsxC}$ particles. These r-proteins are located at the base

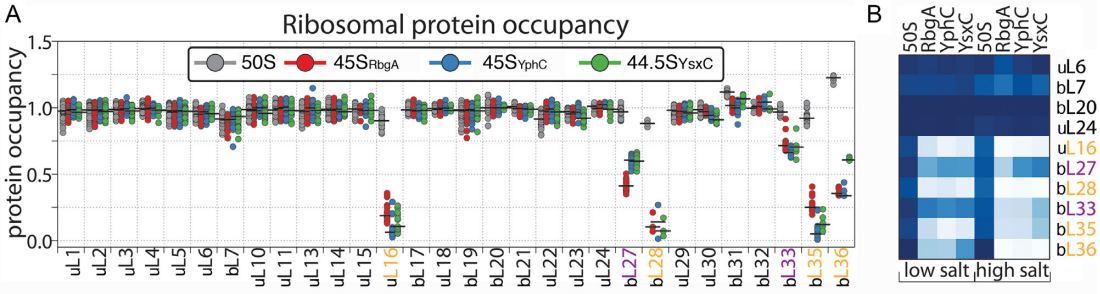

Figure 1. Ribosomal protein occupancy measured by qMS. (**A**) Ribosomal protein occupancy in 50S (gray), $45S_{RbgA}$ (red), $45S_{YphC}$ (blue) and $44.5S_{YsxC}$ (green) particles purified in the presence of 150 mM NH_4Cl. MRM-like transitions were extracted for each product ion from the SWATH datasets (see methods) and $^{14}N/^{15}N$ abundance ratios were calculated and normalized to the median value determined for protein L20. Circles denote individual MRM-transition measurements, lines signify the median $^{14}N/^{15}N$ abundance ratio measured for each protein. (**B**) Protein occupancy for a subset of ribosomal proteins measured in particles purified in the presence of either 150 mM (low salt; left) or 500 mM (high salt; right) NH_4Cl. Occupancy from 0 to 1 scales from white to blue.

of the central protuberance (Figure 2C). In addition, there were six other r-proteins that were present at ∼100% occupancy according to qMS (Figure 1), however density corresponding to these proteins was partially or completely missing from the cryo-EM maps (Figure 2A). These r-proteins were uL6, uL10, uL11 in the bL7/L12 stalk and uL5, bL31 and uL18 in the central protuberance (Figure 2D).

The cryo-EM maps obtained for these classes had a mean resolution of 6.5 Å ($45S_{YphC}$), 5.8 Å ($44.5S_{YsxC}$, class I) and 6.2 Å ($44.5S_{YsxC}$, class II) (Supplementary Figure S4A) with local resolution calculations indicating that the resolution of the core of the immature particles is higher than these values (Supplementary Figures S4B and S4C). This is consistent with the features of the cryo-EM maps in these regions showing clear separation of α-helices and β-sheets in the r-proteins (Supplementary Figure S5A) and the pitch of the rRNA helices (Supplementary Figure S5B). Instead, regions of the cryo-EM maps still in an immature state (central protuberance and functional sites) (Supplementary Figure S4B and S4C) refined to resolutions values lower than the mean resolution of the cryo-EM maps. The non-homogenous resolution likely reflects the stable conformation of the core of these particles, already in the mature conformation, and the relatively flexible nature of the central protuberance and functional sites, which are yet to reach the mature conformation. These maps constitute the highest-resolution structures available to date for a bacterial immature ribosomal particle.

Overall, we found that depletion of YphC or YsxC led to the accumulation of particles that have areas of the central protuberance, L7/12 stalk and functional sites still in an immature conformation. Therefore, we concluded that YphC or YsxC are involved in the maturation of these functional sites, which occur at the late stages of assembly of the 50S subunit. This function is similar to that suggested for RbgA (19,20).

Essential helices in the A, P and E sites of the 50S subunit adopt an immature state in the $45S_{YphC}$ and $44.5S_{YsxC}$ particles

The resolution at which the maps for the $45S_{YphC}$ and $44.5S_{YsxC}$ particles were obtained using the direct detector camera was sufficient to identify clearly the individual rRNA helices that differed from those of the mature 50S subunit in these structures.

The first and most important group of helices that were different in the $45S_{YphC}$ and $44.5S_{YsxC}$ immature particles were those involved in the binding of the tRNA in the A, P and E sites. Densities for helix 89 and for helices 91–93, which are part of the A and P sites were not observed in the cryo-EM maps (Figure 3A and Supplementary Figure S6). Similarly, helix 71 in the P site and the long helix 68, a major structural component of the E site, also did not exhibit a correspondent density (Figure 3B and Supplementary Figure S6). Interestingly, these helices were completely absent in the cryo-EM maps suggesting that they are still flexible and adopt multiple conformations within the population of individual particles.

Helix 69 is another functionally important motif located in the P site and in the immature particles also diverges structurally from the mature 50S subunit (Figure 3B). This helix mediates the essential B2a intersubunit bridge, where helix 69 contacts the decoding site of the 30S subunit. A density for helix 69 is apparent in the $44.5S_{YsxC}$ class I and class II maps, however this helix was bent outward from the mature position by ∼30° (Figure 3B, lower panels, asterisks). This non-native conformation of the helix likely prevents the premature association of the immature particles with the 30S subunit.

Overall, the structural divergence found in the A, P and E sites in the $45S_{YphC}$ and $44.5S_{YsxC}$ particles with respect to the mature 50S subunits most likely prevents these particles from becoming prematurely engage in translation. The obtained structures suggest they are likely to be defective in tRNA binding and in their ability to associate to the 30S subunit. Furthermore, these maps demonstrate that the $45S_{YphC}$ and $44.5S_{YsxC}$ particles have not structurally reached the mature state.

Maturation dependencies between the central protuberance, helix 38 and the GTPase associated region

In addition to the RNA helices forming the A, P and E sites, the $45S_{YphC}$ and $44.5S_{YsxC}$ particles also presented structural differences with the mature subunit in three other important functional domains. These regions were the central

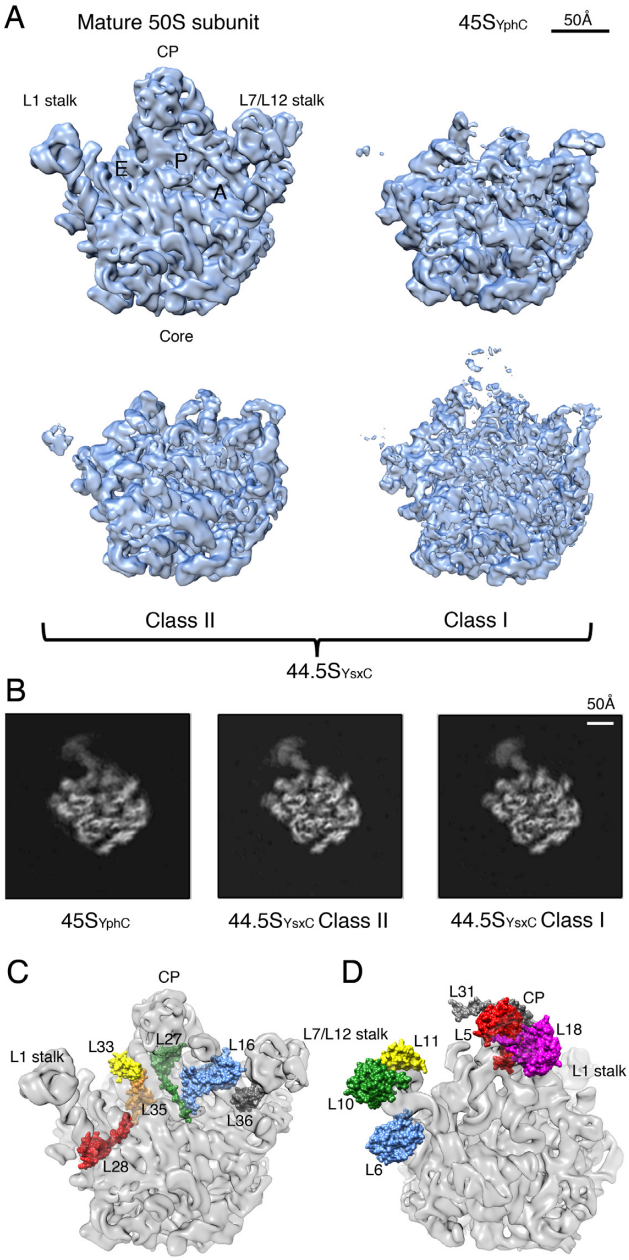

Figure 2. Cryo-EM maps of the 45S$_{YphC}$ and 44.5S$_{YsxC}$ ribosomal particles. (**A**) Surface rendered views of the maps show that the 45S$_{YphC}$ particle was present in one conformational state, whereas the 44.5S$_{YsxC}$ particles exhibited two. The map for the mature 50S subunit was obtained from the 3.9 Å resolution cryo-EM structure of the 50S subunit from *B. subtilis* (PDB ID: 3j9w) by applying a low-pass filter at comparable resolution. Landmarks in the 50S subunit are labeled in the mature subunit. CP stands for central protuberance. (**B**) Cross-sections through the three-dimensional map of the 45S$_{YphC}$ particle and the two conformational states of the 44.5S$_{YsxC}$ particle. (**C**) Location in the 50S subunit mature structure of the ribosomal proteins that were found severely depleted or absent in the 45S$_{YphC}$ and 44.5S$_{YsxC}$ particles. (**D**) The six ribosomal proteins displayed in the structure of the 50S subunit were found to be present at ∼100% occupancy by qMS, but a corresponding density for these proteins was not observed in the 45S$_{YphC}$ and 44.5S$_{YsxC}$ maps.

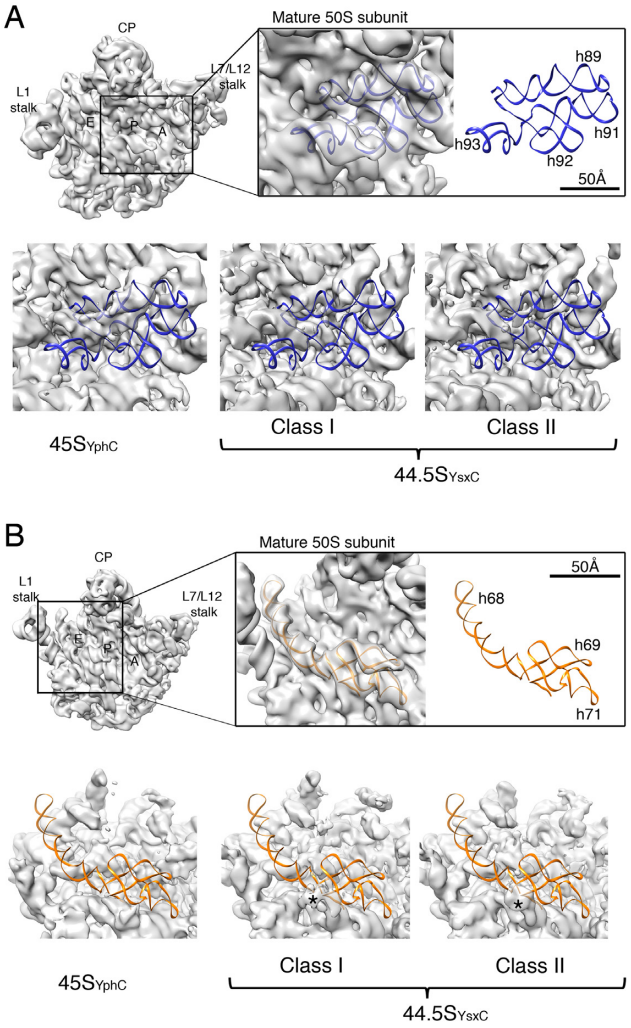

Figure 3. Structure of the functional core of the 45S$_{YphC}$ and 44.5S$_{YsxC}$ immature particles. (**A**) Zoomed view of helices 89–93 in the A site of the 50S subunit. A ribbon representation of these helices (PDB ID: 3j9w) was fitted into the map of the mature 50S subunit (top panel) and the 45S$_{YphC}$ and 44.5S$_{YsxC}$ immature particles (bottom panel). (**B**) This panel shows the structural details of the P and E sites in the immature particles and how they compare with the mature 50S subunit. The indicated helices differ structurally from the mature structure.

protuberance, helix 38 and the GTPase associated region (Supplementary Figure S6).

The central protuberance appeared at a different assembly stage in the obtained 45S$_{YphC}$ and 44.5S$_{YsxC}$ structures. However, none of the maps exhibited a fully assembled central protuberance (Figure 2A). This motif is comprised of helices 80–88 from domain V in the 23S rRNA (Supplementary Figure S6). These helices form the bulk of the central protuberance, whereas the 5S rRNA forms its back. In the maps obtained for the 45S$_{YphC}$ and 44.5S$_{YsxC}$ class II particles, densities for both helices 80–88 and 5S rRNA were missing. However, in the map of the 44.5S$_{YsxC}$ class I, some disconnected densities were apparent for these regions. Similarly, the amount of density representing helix 38 and helices 42–44 comprising the GTPase associated region were

also featuring variable amounts of density among the obtained structures (Figure 2A).

To better understand the conformational changes that these important functional domains undergo during the late stages of assembly, we performed focus classification with the three sets of particle images that generated the $45S_{YphC}$, $44.5S_{YsxC}$ class I and $44.5S_{YsxC}$ class II consensus cryo-EM maps. To this end, we kept the signal in the particle images corresponding to the central protuberance, helix 38, GTPase associated region and helices forming the A, P and E functional sites during the 3D classification. In addition, the signal from all ribosomal motifs that had already reached the mature state was masked out and subtracted from the particle images (29). Each data set rendered three distinct classes with a resolution range of 8–10 Å for $44.5S_{YsxC}$ particle (Supplementary Figure S7) and 9–14 Å for the $45S_{YphC}$ particle (Supplementary Figure S8). These maps still allowed for unequivocal identification of rRNA helices (Figure 4).

Comparison of the three structures identified from the data set producing the consensus $44.5S_{YsxC}$ class I structure revealed that the rRNA helices forming the A, P and E site were consistently not present in any of the maps. However, the other immature regions including the central protuberance, helix 38 and the GTPase associated region (helix 42–44) presented variations (Figure 4A and B). The first class ($44.5S_{YsxC}$ class Ia) did not show density for any of these regions. The second class ($44.5S_{YsxC}$ class Ib) had density present for helix 42 and most of helices 43–44. It also displayed density for the proximal part of helix 38, although the direction of this helix deviated by ∼30° from the mature conformation. There was also no density for helices 80–88 or 5S rRNA indicating that the central protuberance is still in an immature state. Finally, the third class showed a fully formed central protuberance and helix 38 and the GTPase associated region was also close to the mature state (Figure 4B).

The data set generating the consensus $44.5S_{YsxC}$ class II structure also produced three structures (Figure 4C). Two of them ($44.5S_{YsxC}$ class IIa and $44.5S_{YsxC}$ class IIb) were identical to the $44.5S_{YsxC}$ class Ia and $44.5S_{YsxC}$ class Ib described above. The third structure ($44.5S_{YsxC}$ class IIc) presented densities similar to the mature structures for helix 38 (proximal region) and helices 42–44 corresponding to the GTPase associated region. In addition, it also featured fragmented densities in the central protuberance corresponding to helices 80–88 and 5S rRNA. This structure likely represents an immature particle in the process of folding the central protuberance. The RNA helices in the A, P and E site were consistently in an immature state in these three maps.

Finally, the data set producing the consensus $45S_{YphC}$ map also produced three structures (Figure 4D). The first structure was similar to $44.5S_{YsxC}$ class Ia and had no density for the central protuberance and helix 38. It only showed incipient densities for the GTPase associated region. The second structure was again equivalent to the $44.5S_{YsxC}$ class Ib with most of the density for the GTPase associated region present and helix 38 density deviated by ∼30° from the mature conformation. The third map presented density for the three regions and in a conformation

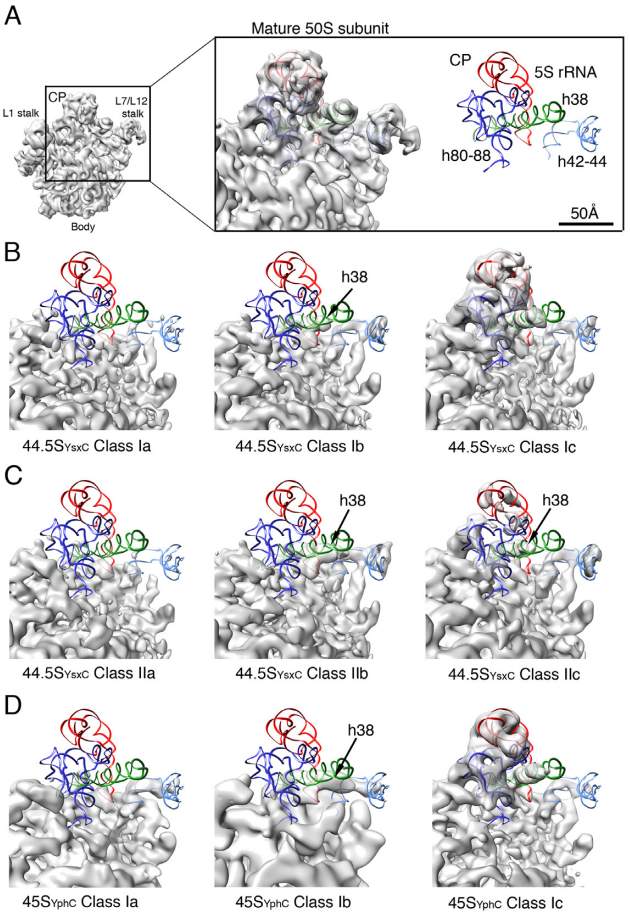

Figure 4. Structure of the central protuberance and GTPase associated region of the $45S_{YphC}$ and $44.5S_{YsxC}$ immature particles. Closed-up views of the central protuberance, helix 38 and the GTPase associated region (helix 42–44) in the cryo-EM maps of the multiple classes obtained from focus classification for the $45S_{YphC}$ (**B**) and (**C**) and $44.5S_{YsxC}$ data sets (**D**). Panel (**A**) shows this region in the mature 50S subunit (PDB ID: 3j9w) and the three bottom panels (B), (C) and (D) in the immature particles. A ribbon representation of helices 80–88, helix 38 and helices 42–44 of the 23S rRNA and 5S rRNA were fitted to the cryo-EM maps. The density representing helix 38 in some of the classes obtained for the $44.5S_{YsxC}$ and $45S_{YphC}$ particles is indicated with a black arrow. The frontal view of the 50S subunit (left) is for orientation purposes and the framed area correspond to the zoomed views in the rest of the panel.

close to the mature state. However, similar to all the other structures it showed fully immature A, P and E sites.

These structural data suggest that the GTPase associated region, helix 38, central protuberance and A, P and E functional sites fold sequentially and in a coordinated manner. It starts with folding of helix 42 and is followed by the other two helices that are part of the GTPase associated region (helix 43–44) adopting the mature conformation. Simultaneously, helix 38 starts extending, however it initially attaches to the particle with an angle different from the mature structure (Movie 1). Subsequently, folding of helices 80–88 and 5S rRNA forming the central protuberance drags helix 38 toward his mature position (Movies 2 and 3). The very last regions to mature are the A, P and E site. The densities corresponding to the RNA helices forming these sites were consistently missing in all the cryo-EM maps obtained

for the $45S_{YphC}$ and $44.5S_{YsxC}$ structure and discrete steps during their maturation were not visualized.

YphC, YsxC and RbgA directly interact with both the mature and immature ribosomal particles

The structural similarities of the $45S_{YphC}$ and $44.5S_{YsxC}$ particles prompted us to test whether YphC and YsxC have the ability to bind to the two assembly intermediates or conversely, whether they only recognize the immature particle that appears upon their depletion. We noticed that the two immature particles analyzed structurally here resemble to that of the $45S_{RbgA}$ particle (19,20). Thus, we also purified $45S_{RbgA}$ particles and the RbgA protein and tested the binding of YphC, YsxC and RbgA to all three immature particles and to mature 50S subunits.

We first used a filtration assays to test the binding of YphC, YsxC and RbgA to the mature 50S subunit and to the three immature ribosomal particles (Figure 5). In these assays, a mixture of the assembly factor with the ribosomal particle was incubated at 37°C for 1 h in the presence of 1 mM GMPPNP. Subsequently, reactions were centrifuged in a centrifugal concentrating device, which retains assembly factor when bound to the ribosome particles and free ribosomal subunits (bound fraction), but passes through the membrane when not bound to ribosomes or free ribosomal subunits (unbound fraction). Both fractions were subsequently analyzed by SDS-PAGE.

We found that none of the three proteins were retained by the filter in the absence of ribosomes, but when combined with the ribosomal particles YsxC exhibited similar binding to both the mature and immature particles (Figure 5C). YphC and RbgA also associated with the immature and mature particles and although the quantitative nature of these assays is limited, we could observe a larger fraction of the protein in the bound fraction for reactions containing the immature particles than for reactions containing the mature 50S subunit (Figure 5A and B). In addition, the filtration assays suggested that a strict hierarchy of binding for these factors or to the ribosomal subunits does not exist.

To determine the effect of the nucleotide on the binding affinity of RbgA, YphC and YsxC to the ribosomal particles, identical reactions were tested in the presence of 1mM GTP or 1mM GDP (Supplementary Figure S9). In the case of RbgA and YphC we found that the binding observed in the presence of these two nucleotides was weaker than in the presence of GMPPNP (Supplementary Figure S9A and S9B). Instead, YsxC showed similar binding to the ribosomal particles with the three nucleotides (Supplementary Figure S9C). These binding results for RbgA are in full agreement with previous literature (16,41,42).

Next, we tested whether the ribosomal particles could simultaneous bind multiple assembly factors. To this end, we performed filtration assays (Figure 5D) where we incubated the ribosomal particles with 5-fold molar excess of each one of the assembly factors and in the presence of 1 mM GMPPNP. These assays revealed that several assembly factors were retained with each of the immature particles and the mature 50S subunit in approximately stoichiometric amounts. This experiment suggested that simultaneous

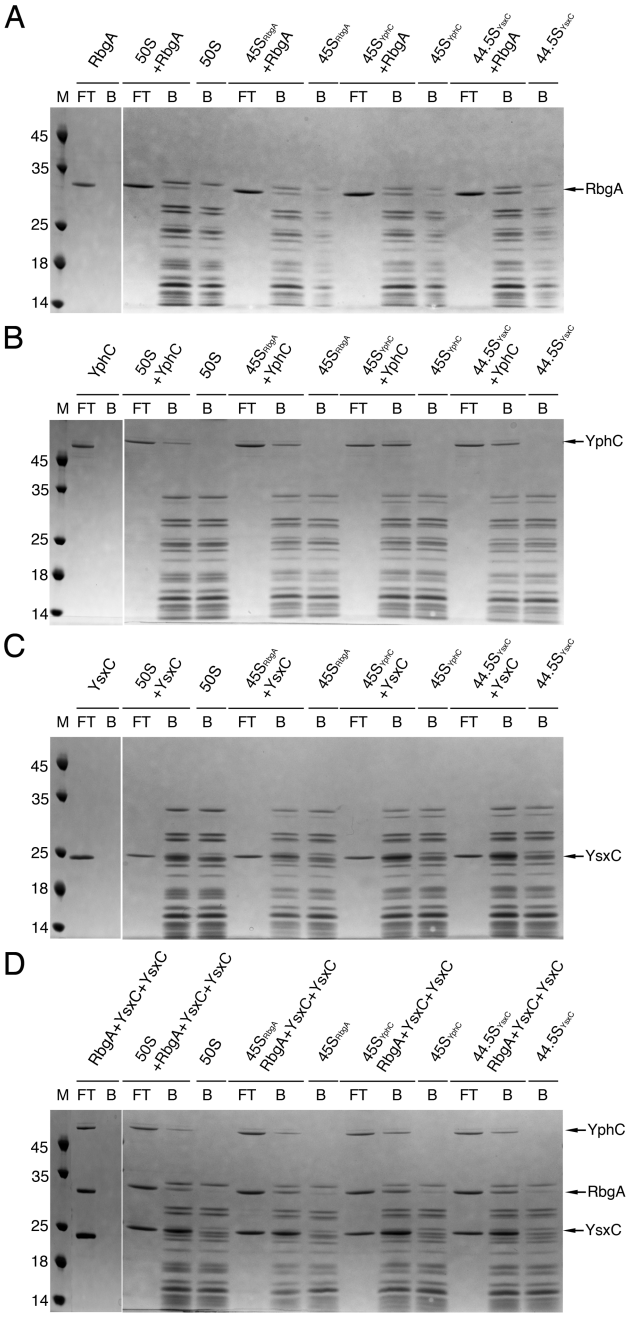

Figure 5. Binding of RbgA, YphC and YsxC to the mature 50S subunit and the $45S_{YphC}$ and $44.5S_{YsxC}$ immature particles. (**A**) Filtration assays testing binding of RbgA to the mature 50S subunit and the $45S_{YphC}$ and $44.5S_{YsxC}$ immature particles. A Coomassie blue stained 4–12% bis–tris polyacrylamide gel shows the content of the flow-through (FT) and bound (**B**) fractions of the filtration assay. Reactions contained RbgA alone or a mixture of ribosomal particles with a five-fold molar excess of RbgA. The molecular weight (M) is in kDa. Similar assay as described in the two panels below showing a similar filtration assay to test the binding of YphC (**B**) or YsxC (**C**) to the mature 50S subunit and the $45S_{YphC}$ and $44.5S_{YsxC}$ immature particles. (**D**) Filtration assay testing binding of multiple assembly factors to the ribosomal particles. In this assay a five-fold molar excess of each factor with respect to the ribosomal particle was added to the assembly reaction.

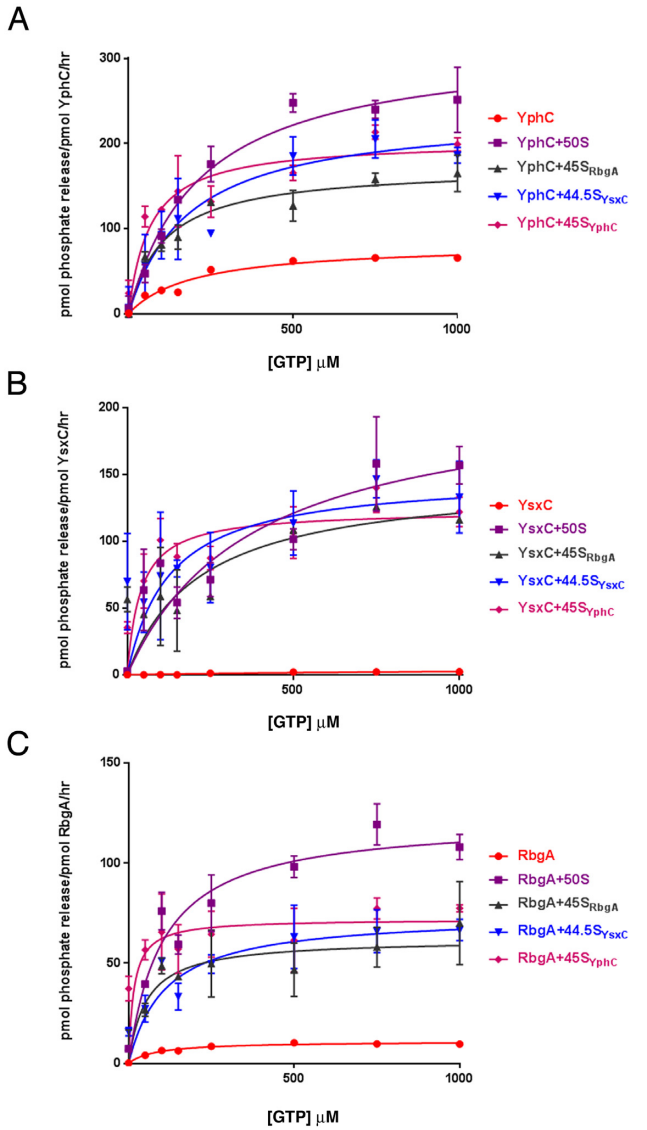

Figure 6. Stimulation of the GTPase activity of YphC, YsxC and RbgA by the mature 50S subunit and immature 45S$_{YphC}$, 45S$_{RbgA}$ and 44.5S$_{YsxC}$ particles. (**A**) The GTP hydrolysis rates of YphC in the presence and absence of the mature and immature ribosomal particles were measured at different concentrations of GTP to determine kinetic parameters. Equivalent experiment with YsxC (**B**) and RbgA (**C**) to determine the kinetic parameters of these enzymes.

binding of more than one of the assembly factors to the mature 50S and immature particles is possible.

RbgA, like most other GTPases exhibits low intrinsic GTPase activity. However, this activity increases upon a specific interaction with the 50S subunit (41,42). We hypothesized that YphC and YsxC may exhibit a similar behavior and measured their GTPase activity in the absence and presence of ribosomal particles to test whether the binding observed in the filtration assays was specific. RbgA was also included in these experiments as a control.

We started by performing a steady-state kinetic analysis of the YphC, YsxC and RbgA intrinsic GTPase activity (Figure 6 and Table 1). The three proteins had low affinity for GTP exhibiting an apparent K_M for this nucleotide in the micromolar range. They also showed a low intrinsic GTP hydrolysis rate. YsxC and RbgA exhibited a k_{cat} of ∼5 and 10 h^{-1}, respectively (Figure 6B and C and Table 1). YphC contains two GTPase domains and it showed a higher rate with a k_{cat} of ∼82 h^{-1} (Figure 6A and Table 1.) These basal levels of GTPase activity were comparable to the k_{cat} reported for RbgA (42) and EngA (43), the ortholog of YphC in *Escherichia coli*.

We then tested the GTPase activity of YphC, YsxC and RbgA in the presence of the mature 50S subunit and the three immature particles (45S$_{YphC}$, 44.5S$_{YsxC}$ and 45S$_{RbgA}$) (Figure 6 and Table 1). The GTPase activity exhibited by each ribosomal particle by itself at each GTP concentration was subtracted. These experiments showed that for the three GTPases a significantly higher stimulation of the catalytic rate of the enzyme against GTP (increase in k_{cat} Table 1) occurred in the presence of the mature 50S subunit. The three immature particles also stimulated the catalytic rate but always to a lesser extent. Overall, the YsxC catalytic rate showed a much higher stimulation (∼26–38-fold) in the presence of the ribosomal particles than in the case of YphC and RbgA (∼2–11-fold).

Interaction with the ribosomal particles also had an effect in the apparent K_M of the enzymes for GTP (Table 1). YphC and RbgA followed a similar pattern exhibiting a small increase in the apparent K_M value in the presence of 50S subunits but a decrease with the immature particles (with the only exception of RbgA in the presence of 44.5S$_{YsxC}$ particle). Instead, YsxC showed a decrease in the apparent K_M value with both mature and immature particles. An interesting observation was that for the three GTPases, the biggest decrease in the apparent K_M value was always observed in the presence of the 44.5S$_{YphC}$ particle. Consequently, we observed an increase in the enzyme efficiency (increase in k_{cat}/apparent K_M Table 1) for all the reactions performed in the presence of ribosomal particles compared to those reactions with the assembly intermediates by themselves. The highest increases in enzyme efficiency were always shown by the reactions of the three GTPases containing the 44.5S$_{YphC}$ particle.

Overall, these results suggest that each one of the GTPases (YphC, YsxC and RbgA) have the ability to bind in a specific manner to both the mature 50S subunit and the three immature ribosomal particles. This finding is consistent with the last steps of assembly of the 50S subunit following multiple parallel pathways of assembly. The observed binding promiscuity of the YphC, YsxC and RbgA GTPases and the fact that a specific binding hierarchy does not exist likely allows for the last steps of maturation of the 50S subunit to occur without following a precise sequence.

DISCUSSION

Inferring the function of YphC and YsxC from the analysis of ribosome assembly intermediates

Recent work (19,20) has described that the RbgA GTPase is involved in the maturation of the central protuberance, tRNA binding sites and GTPase associating region. Here, we describe that two additional GTPases, YphC and YsxC

Table 1. Kinetic parameters of YphC, YsxC and RbgA in the presence and absence of the mature 50S subunit and immature $45S_{YphC}$, $45S_{RbgA}$ and $44.5S_{YsxC}$ particles

	Apparent K_M (μM)	k_{cat} (h^{-1})	k_{cat}/apparent K_M (μM^{-1} h^{-1})	Increase in apparent K_M	Increase in k_{cat}	Increase in k_{cat}/apparent K_M
YphC	199 ± 31.4	82.2 ± 4.3	0.41	1	1	1
YphC+50S	217.4 ± 39.2	317.9 ± 19.2	1.4	1.1	3.9	3.5
YphC+45SYphC	64.5 ± 18.9	203.3 ± 13.1	3.1	0.3	2.5	7.7
YphC+45SRbgA	108.3 ± 21.2	172.4 ± 9.3	1.5	0.5	2.1	3.9
YphC+44.5SYsxC	185.3 ± 57.4	236.5 ± 24.6	1.2	0.9	2.9	3.1
YsxC	1268 ± 116.6	5.5 ± 3.3	0.004	1	1	1
YsxC +50S	377.1 ± 166.7	212.3 ± 40.9	0.5	0.3	38.1	128.1
YsxC +45SYphC	39.5 ± 18.4	123 ± 9.6	3.1	0.03	22.1	707.9
YsxC +45SRbgA	219.6 ± 174.6	147.6 ± 45.5	0.6	0.2	26.5	153
YsxC +44.5SYsxC	126.3 ± 72.5	149 ± 25.3	1.1	0.1	26.7	268.5
RbgA	82.8 ± 9.4	10.9 ± 0.3	0.1	1	1	1
RbgA +50S	102.8 ± 24.4	121.7 ± 6.9	1.2	1.2	11.1	8.9
RbgA +45SYphC	15.5 ± 16	72 ± 7.5	4.6	0.2	6.6	35
RbgA +45SRbgA	53.4 ± 21.6	61.9 ± 5.2	1.2	0.6	5.6	8.8
RbgA +44.5SYsxC	110.5 ± 36.7	74.2 ± 6.3	0.7	1.3	6.8	5.1

also contribute in the maturation of these essential ribosomal motifs.

Interestingly, we found that the $45S_{YphC}$ and $44.5S_{YsxC}$ particles that accumulate in *B. subtilis* strains upon depletion of YphC and YsxC are structurally similar to each other and also resemble the $45S_{RbgA}$ particles that result from the depletion of RbgA (19,20). From the analysis of the immature regions in the cryo-EM maps, it is still difficult to pinpoint specific roles for RbgA, YphC and YsxC during the assembly of the 50S subunit.

Identification of structurally divergent intermediates would have been the expected outcome if each one of the factors performs a distinct function not related to the function of other factors. Instead, we found that the cryo-EM maps of the $45S_{YphC}$, $44.5S_{YsxC}$ and $45S_{RbgA}$ particles were similar. One possibility consistent with this result is that RbgA, YphC and YsxC work in conjunction during the maturation of the central protuberance, helix 38, GTPase associated region and A, P and E functional sites and thus, removing any of the factors leads to accumulation of the same intermediate. However, similar intermediate structures would also be expected if depletion of each one of these factors blocks the assembly at a different step and leads to the accumulation of a different thermodynamically unstable intermediate that evolves into a similar energetically stable conformation. Consequently, a related and relevant question is whether these particles are on-pathway and whether they represent the actual substrate for the assembly factors.

We recently demonstrated that the $45S_{RbgA}$ particles are competent for maturation and are eventually incorporated into 70S ribosomes (19). In addition, the work presented here reveals that the $45S_{YphC}$, $44.5S_{YsxC}$ and $45S_{RbgA}$ particles specifically bind YphC, YsxC and RbgA suggesting that they either constitute actual on-pathway intermediates or their conformations have not diverged significantly from the actual substrate recognized by the assembly factors. Therefore, the structural differences existing in these immature particles compared to the mature 50S subunit should be informative of the function of the assembly factors.

High resolution cryo-EM structures provides precise testable models about YphC and YsxC function

The presented structures were obtained using a direct electron detector and were refined to a resolution of 5–6 Å. They constitute to our knowledge the highest resolution cryo-EM structures available for a bacterial ribosome intermediate. Therefore, different from previous moderate-resolution cryo-EM studies on other assembly intermediates (11–13,15,19,20), these structures allow defining individual rRNA helices in the $45S_{YphC}$ and $44.5S_{YsxC}$ particles that are still adopting an immature conformation. Consequently, these structures are making possible to propose precise testable models regarding the function of YphC and YsxC in assembly. For example, Li *et al.* (20) assigned RbgA a role as an rRNA chaperone with the essential role of positioning helix 38 during 50S subunit maturation. The structures presented here indicate that helix 38 is able to adopt its mature conformation in the absence of YphC or YsxC (Movies 1–3). Similarly, our results also indicate that YphC and YsxC are not essential for the assembly of the central protuberance and GTPase associated center. However, the RNA helices forming the A, P and E site consistently appear in an immature state in the $45S_{YphC}$, $44.5S_{YsxC}$ structures (Figure 3), thus suggesting that the essential role of YphC and YsxC may be more related to the remodeling of the RNA helices in the functional core of the particle. Consistent with this proposed function, a recent high-resolution structure of EngA, the *Escherichia coli* homologue of YphC, in complex with the mature 50S subunit (44) revealed that this factor binds deeply into the tRNA passage at the P and E site. Interestingly, binding of EngA results in significant rearrangements of the same rRNA helices (helix 68–71) that we found still in an immature state in the $45S_{YphC}$, $44.5S_{YsxC}$ particles.

The high resolution obtained in the cryo-EM maps also provides a structural explanation to deficiencies found in the protein complement of these particles. For example, the cryo-EM maps for the $44.5S_{YsxC}$ class Ib, $44.5S_{YsxC}$ class IIb and the $45S_{YphC}$ class Ib particles, the position of helix 38 completely blocks the binding site of uL16. Only when the central protuberance is formed, helix 38 is dragged closed

to its mature position making the uL16 binding site accessible and providing a justification for the almost complete absence of uL16 found in the $44.5S_{YsxC}$ and $45S_{YphC}$ particles. The abnormal positioning of helix 38 and steric blockage of the uL16 binding site is a structural feature of the $44.5S_{YsxC}$ and $45S_{YphC}$ particles shared with the cryo-EM map of the $45S_{RbgA}$ particles that was described recently (19,20).

Certain features of the cryo-EM maps of the $45S_{YphC}$ and $44.5S_{YsxC}$ particles are in full agreement with the assembly of the ribosomal particle following multiple parallel pathways of assembly (45–48). In particular, we found that there were not densities in these maps representing the RNA helices comprising the A, P and E sites at the site for the mature 50S subunit or nearby (Figure 3). This finding suggests that these rRNA motifs probably adopt a large number of conformations that are those populating the multiple assembly pathways undergoing in the cell. In addition, as described for the $45S_{RbgA}$ particles (19,20) these structures are also consistent with the folding of the 23S rRNA not proceeding in 5′-3′ fashions, as domains II, IV and V are still in an immature state. However, all other domains including I, III and VI already reached the mature stage (Supplementary Figure S6). This is in contrast to the assembly of the 16S rRNA forming the 30S subunit where the rRNA folding follows and strict 5′-3′ transcriptional order (49).

Cryo-EM allows for direct visualization of the ribosomal assembly process

The $45S_{YphC}$ and $44.5S_{YsxC}$ cryo-EM maps also describe the discrete stages leading to the coordinated assembly of functional important sites for the 50S subunit, including the GTPase associated center, helix 38 and central protuberance (Movies 1–3). It starts with the helix 42 reaching its mature conformation and followed by the folding of helix 43–44, which are the other two helices comprising the GTPase associated region. At this moment helix 38 start to grow, however it initially attaches to the ribosomal particle with a different angle. As helices 80–88 and 5S rRNA forming the central protuberance start to fold simultaneously, helix 38 is dragged towards its mature position. Two of the conformations observed for the central protuberance (classes I and II of the $44.5S_{YsxC}$ particle) had also much resemblance with two of the conformational classes that have been described for the $45S_{RbgA}$ immature particle (19,20). These results suggest that although the assembly of the central protuberance follow multiple parallel pathways, the conformational variability existing among the population of assembling particles may not be as diverse as it has been observed for the RNA motifs comprising A, P and E sites where discrete conformations were not observed.

These structures also suggest that the assembly of the central protuberance in the bacterial ribosome occurs differently than in the eukaryotic ribosome. A recent study (50) revealed the existence of an energetically favored intermediate of the 60S ribosomal subunit with a drastically rearranged topology of the central protuberance. Compared to its mature position, the 5S rRNA, an integral part of the central protuberance exhibits an essentially unchanged fold but the entire molecule is rotated by 180°. This non-native conformation is stabilized by assembly factors Rsa4 and Nog1. In subsequent maturation steps, the 5S rRNA rotates to its native position and for this movement it is predicted that one of the assembly factors will have to provide a substantial power stroke. During the late stages of assembly of the bacterial 50S subunit studied here, we did not observed assembly intermediates exhibiting a central protuberance with a rearranged topology.

CONCLUSION

Overall, these results provide the first insights into the function of YphC and YsxC at the late stages of assembly of the 50S subunit. Ribosome assembly intermediates generated through depletion and knock-out bacterial strains constitute today an important tool for studying the function of assembly factors. Therefore, the key questions answered here regarding the nature of these intermediates and their ability to inform on the reactions catalyzed by assembly factors constitute an important step forward toward our understanding of the ribosome assembly process.

ACCESION NUMBERS

The $44.5S_{YsxC}$ class I and class II cryo-EM maps have been assigned the EMDB IDs 8274 and 8275, respectively. The EMDB ID for the $45S_{YphC}$ cryo-EM map is 8276.

SUPPLEMENTARY DATA

Supplementary Data are available at NAR Online.

ACKNOWLEDGEMENTS

We are grateful to Dr Brandon Aubie for technical assistance with the MSLR computing cluster. We acknowledge the Hospital for Sick Children in Toronto for allowing us access to the Electron Microscopy Facility. Canadian Institutes of Health Research provided the funds for open access charges.

FUNDING

National Science and Engineering Research Council of Canada [RGPIN288327-07]; Canadian Institutes of Health Research [MOP-82930 to J.O.]; Canadian Institutes of Health Research [MOP-81294]; Canada Research Chair funding (to J.L.R.); National Institutes of Health [R01GM110248 to to R.A.B. and J.R.W.]; The McMaster Service Lab and Repository (MSLR) computing cluster was, in part, funded by a grant from the Canadian Foundation for Innovation (to A.G.M.). A.G.M. holds a Cisco Research Chair in Bioinformatics, supported by Cisco Systems Canada, Inc.; Jane Coffin Childs Postdoctoral fellowship and a grant from the National Institute of Aging [1K99AG050749-01 to J.H.D.]. Funding for open access charge: Canadian Institutes of Health Research.
Conflict of interest statement. None.

REFERENCES

1. Lindahl,L. (1973) Two new ribosomal precursor particles in E. coli. *Nat. New Biol.*, **243**, 170–172.

2. Lindahl,L. (1975) Intermediates and time kinetics of the in vivo assembly of Escherichia coli ribosomes. *J. Mol. Biol.*, **92**, 15–37.
3. Hayes,F. and Hayes,D.H. (1971) Biosynthesis of ribosomes in E. coli. I. Properties of ribosomal precursor particles and their RNA components. *Biochimie*, **53**, 369–382.
4. Stokes,J.M. and Brown,E.D. (2015) Chemical modulators of ribosome biogenesis as biological probes. *Nat. Chem. Biol.*, **11**, 924–932.
5. Loibl,M., Klein,I., Prattes,M., Schmidt,C., Kappel,L., Zisser,G., Gungl,A., Krieger,E., Pertschy,B. and Bergler,H. (2014) The drug diazaborine blocks ribosome biogenesis by inhibiting the AAA-ATPase Drg1. *J. Biol. Chem.*, **289**, 3913–3922.
6. Pertschy,B., Zisser,G., Schein,H., Koffel,R., Rauch,G., Grillitsch,K., Morgenstern,C., Durchschlag,M., Hogenauer,G. and Bergler,H. (2004) Diazaborine treatment of yeast cells inhibits maturation of the 60S ribosomal subunit. *Mol. Cell. Biol.*, **24**, 6476–6487.
7. Drygin,D., Lin,A., Bliesath,J., Ho,C.B., O'Brien,S.E., Proffitt,C., Omori,M., Haddach,M., Schwaebe,M.K., Siddiqui-Jain,A. *et al.* (2011) Targeting RNA polymerase I with an oral small molecule CX-5461 inhibits ribosomal RNA synthesis and solid tumor growth. *Cancer Res.*, **71**, 1418–1430.
8. Drygin,D., Siddiqui-Jain,A., O'Brien,S., Schwaebe,M., Lin,A., Bliesath,J., Ho,C.B., Proffitt,C., Trent,K., Whitten,J.P. *et al.* (2009) Anticancer activity of CX-3543: a direct inhibitor of rRNA biogenesis. *Cancer Res.*, **69**, 7653–7661.
9. Deisenroth,C. and Zhang,Y. (2010) Ribosome biogenesis surveillance: probing the ribosomal protein-Mdm2-p53 pathway. *Oncogene*, **29**, 4253–4260.
10. Stokes,J.M., Davis,J.H., Mangat,C.S., Williamson,J.R. and Brown,E.D. (2014) Discovery of a small molecule that inhibits bacterial ribosome biogenesis. *eLife*, **3**, e03574.
11. Jomaa,A., Stewart,G., Martin-Benito,J., Zielke,R., Campbell,T.L., Maddock,J.R., Brown,E.D. and Ortega,J. (2011) Understanding ribosome assembly: the structure of in vivo assembled immature 30S subunits revealed by cryo-electron microscopy. *RNA*, **17**, 697–709.
12. Leong,V., Kent,M., Jomaa,A. and Ortega,J. (2013) Escherichia coli rimM and yjeQ null strains accumulate immature 30S subunits of similar structure and protein complement. *RNA*, **19**, 789–802.
13. Guo,Q., Goto,S., Chen,Y., Feng,B., Xu,Y., Muto,A., Himeno,H., Deng,H., Lei,J. and Gao,N. (2013) Dissecting the in vivo assembly of the 30S ribosomal subunit reveals the role of RimM and general features of the assembly process. *Nucleic Acids Res.*, **41**, 2609–2620.
14. Clatterbuck Soper,S.F., Dator,R.P., Limbach,P.A. and Woodson,S.A. (2013) In vivo X-ray footprinting of pre-30S ribosomes reveals chaperone-dependent remodeling of late assembly intermediates. *Mol. Cell*, **52**, 506–516.
15. Yang,Z., Guo,Q., Goto,S., Chen,Y., Li,N., Yan,K., Zhang,Y., Muto,A., Deng,H., Himeno,H. *et al.* (2014) Structural insights into the assembly of the 30S ribosomal subunit in vivo: functional role of S5 and location of the 17S rRNA precursor sequence. *Protein Cell*, **5**, 394–407.
16. Uicker,W.C., Schaefer,L. and Britton,R.A. (2006) The essential GTPase RbgA (YlqF) is required for 50S ribosome assembly in Bacillus subtilis. *Mol. Microbiol.*, **59**, 528–540.
17. Schaefer,L., Uicker,W.C., Wicker-Planquart,C., Foucher,A.E., Jault,J.M. and Britton,R.A. (2006) Multiple GTPases participate in the assembly of the large ribosomal subunit in Bacillus subtilis. *J. Bacteriol.*, **188**, 8252–8258.
18. Hwang,J. and Inouye,M. (2006) The tandem GTPase, Der, is essential for the biogenesis of 50S ribosomal subunits in Escherichia coli. *Mol. Microbiol.*, **61**, 1660–1672.
19. Jomaa,A., Jain,N., Davis,J.H., Williamson,J.R., Britton,R.A. and Ortega,J. (2014) Functional domains of the 50S subunit mature late in the assembly process. *Nucleic Acids Res.*, **42**, 3419–3435.
20. Li,N., Chen,Y., Guo,Q., Zhang,Y., Yuan,Y., Ma,C., Deng,H., Lei,J. and Gao,N. (2013) Cryo-EM structures of the late-stage assembly intermediates of the bacterial 50S ribosomal subunit. *Nucleic Acids Res.*, **41**, 7073–7083.
21. Uicker,W.C., Schaefer,L., Koenigsknecht,M. and Britton,R.A. (2007) The essential GTPase YqeH is required for proper ribosome assembly in Bacillus subtilis. *J. Bacteriol.*, **189**, 2926–2929.
22. Jeganathan,A., Razi,A., Thurlow,B. and Ortega,J. (2015) The C-terminal helix in the YjeQ zinc-finger domain catalyzes the release of RbfA during 30S ribosome subunit assembly. *RNA*, **21**, 1203–1216.
23. MacLean,B., Tomazela,D.M., Shulman,N., Chambers,M., Finney,G.L., Frewen,B., Kern,R., Tabb,D.L., Liebler,D.C. and MacCoss,M.J. (2010) Skyline: an open source document editor for creating and analyzing targeted proteomics experiments. *Bioinformatics*, **26**, 966–968.
24. Gillet,L.C., Navarro,P., Tate,S., Rost,H., Selevsek,N., Reiter,L., Bonner,R. and Aebersold,R. (2012) Targeted data extraction of the MS/MS spectra generated by data-independent acquisition: a new concept for consistent and accurate proteome analysis. *Mol. Cell. Proteomics*, **11**, doi:10.1074/mcp.O111.016717.
25. Gulati,M., Jain,N., Davis,J.H., Williamson,J.R. and Britton,R.A. (2014) Functional interaction between ribosomal protein L6 and RbgA during ribosome assembly. *PLoS Genet.*, **10**, e1004694.
26. Rubinstein,J.L. and Brubaker,M.A. (2015) Alignment of cryo-EM movies of individual particles by optimization of image translations. *J. Struct. Biol.*, **192**, 188–195.
27. Mindell,J.A. and Grigorieff,N. (2003) Accurate determination of local defocus and specimen tilt in electron microscopy. *J. Struct. Biol.*, **142**, 334–347.
28. Scheres,S.H. (2012) RELION: implementation of a Bayesian approach to cryo-EM structure determination. *J. Struct. Biol.*, **180**, 519–530.
29. Bai,X.C., Rajendra,E., Yang,G., Shi,Y. and Scheres,S.H. (2015) Sampling the conformational space of the catalytic subunit of human gamma-secretase. *eLife*, **4**, e11182.
30. Rosenthal,P.B. and Henderson,R. (2003) Optimal determination of particle orientation, absolute hand, and contrast loss in single-particle electron cryomicroscopy. *J. Mol. Biol.*, **333**, 721–745.
31. Loken,C., Gruner,D., Groer,L., Peltier,R., Bunn,N., Craig,M., Henriques,T., Dempsey,J., Yu,C.-H., Chen,J. *et al.* (2010) SciNet: Lessons Learned from Building a Power-efficient Top-20 System and Data Centre. *J. Phys.*, **256**, 012026.
32. Kucukelbir,A., Sigworth,F.J. and Tagare,H.D. (2014) Quantifying the local resolution of cryo-EM density maps. *Nat. Methods*, **11**, 63–65.
33. Pettersen,E.F., Goddard,T.D., Huang,C.C., Couch,G.S., Greenblatt,D.M., Meng,E.C. and Ferrin,T.E. (2004) UCSF Chimera–a visualization system for exploratory research and analysis. *J. Comput. Chem.*, **25**, 1605–1612.
34. Trabuco,L.G., Villa,E., Mitra,K., Frank,J. and Schulten,K. (2008) Flexible fitting of atomic structures into electron microscopy maps using molecular dynamics. *Structure*, **16**, 673–683.
35. Ban,N., Beckmann,R., Cate,J.H., Dinman,J.D., Dragon,F., Ellis,S.R., Lafontaine,D.L., Lindahl,L., Liljas,A., Lipton,J.M. *et al.* (2014) A new system for naming ribosomal proteins. *Curr. Opin. Struct. Biol.*, **24**, 165–169.
36. Rohl,R. and Nierhaus,K.H. (1982) Assembly map of the large subunit (50S) of Escherichia coli ribosomes. *Proc. Natl. Acad. Sci. U.S.A.*, **79**, 729–733.
37. Herold,M. and Nierhaus,K.H. (1987) Incorporation of six additional proteins to complete the assembly map of the 50 S subunit from Escherichia coli ribosomes. *J. Biol. Chem.*, **262**, 8826–8833.
38. Chen,S.S. and Williamson,J.R. (2013) Characterization of the ribosome biogenesis landscape in E. coli using quantitative mass spectrometry. *J. Mol. Biol.*, **425**, 767–779.
39. Nomura,M. and Erdmann,V.A. (1970) Reconstitution of 50S ribosomal subunits from dissociated molecular components. *Nature*, **228**, 744–748.
40. Fahnestock,S., Erdmann,V. and Nomura,M. (1973) Reconstitution of 50S ribosomal subunits from protein-free ribonucleic acid. *Biochemistry*, **12**, 220–224.
41. Matsuo,Y., Morimoto,T., Kuwano,M., Loh,P.C., Oshima,T. and Ogasawara,N. (2006) The GTP-binding protein YlqF participates in the late step of 50 S ribosomal subunit assembly in Bacillus subtilis. *J Biol Chem*, **281**, 8110–8117.
42. Achila,D., Gulati,M., Jain,N. and Britton,R.A. (2012) Biochemical characterization of ribosome assembly GTPase RbgA in Bacillus subtilis. *J. Biol. Chem.*, **287**, 8417–8423.
43. Bharat,A., Jiang,M., Sullivan,S.M., Maddock,J.R. and Brown,E.D. (2006) Cooperative and critical roles for both G domains in the GTPase activity and cellular function of ribosome-associated Escherichia coli EngA. *J. Bacteriol.*, **188**, 7992–7996.
44. Zhang,X., Yan,K., Zhang,Y., Li,N., Ma,C., Li,Z., Zhang,Y., Feng,B., Liu,J., Sun,Y. *et al.* (2014) Structural insights into the function of a

unique tandem GTPase EngA in bacterial ribosome assembly. *Nucleic Acids Res.*, **42**, 13430–13439.
45. Shajani,Z., Sykes,M.T. and Williamson,J.R. (2011) Assembly of bacterial ribosomes. *Annu. Rev. Biochem.*, **80**, 501–526.
46. Sykes,M.T. and Williamson,J.R. (2009) A Complex Assembly Landscape for the 30S Ribosomal Subunit. *Annu. Rev. Biophys.*, **38**, 197–215.
47. Woodson,S.A. (2008) RNA folding and ribosome assembly. *Curr. Opin. Chem. Biol.*, **12**, 667–673.
48. Woodson,S.A. (2011) RNA folding pathways and the self-assembly of ribosomes. *Acc. Chem. Res.*, **44**, 1312–1319.
49. Mulder,A.M., Yoshioka,C., Beck,A.H., Bunner,A.E., Milligan,R.A., Potter,C.S., Carragher,B. and Williamson,J.R. (2010) Visualizing ribosome biogenesis: parallel assembly pathways for the 30S subunit. *Science*, **330**, 673–677.
50. Leidig,C., Thoms,M., Holdermann,I., Bradatsch,B., Berninghausen,O., Bange,G., Sinning,I., Hurt,E. and Beckmann,R. (2014) 60S ribosome biogenesis requires rotation of the 5S ribonucleoprotein particle. *Nat. Commun.*, **5**, 3491.